Optical Materials 99 (2020) 109579

Contents lists available at ScienceDirect

Optical Materials

journal homepage: http://www.elsevier.com/locate/optmat

Study of the influence of Er/Ln co-doping in La_2O_3 thin films on their up-conversion properties (where Ln = Ho or Nd)

G. Cabello-Guzmán [a,*], C. Caro-Díaz [a], A. Fernandez-Perez [b], G.E. Buono-Core [c], B. Chornik [d]

[a] Departamento de Ciencias Básicas, Facultad de Ciencias, Universidad del Bío-Bío, Chillán, Chile
[b] Departamento de Física, Facultad de Ciencias, Universidad del Bío-Bío, Concepción, Chile
[c] Instituto de Química, Pontificia Universidad Católica de Valparaíso, Valparaíso, Chile
[d] Deparamento de Física, Facultad de Ciencias Físicas y Matemáticas, Universidad de Chile, Santiago, 8370415, Chile

ARTICLE INFO

Keywords:
Thin films
Photochemical deposition
Up-conversion emission
Energy transfer

ABSTRACT

In this study we report significant enhancement of up-conversion emissions of La_2O_3:Er thin films when they are co-doped with Er/Ln (where Ln = Nd or Ho). The proposed mechanisms by which the Ln ions contribute to these emissions are based on different mechanistic routes. While the La_2O_3 samples co-doped with Er/Nd involves energy transfer $Nd^{III} \rightarrow Er^{III}$ processes, in the La_2O_3 samples co-doped with Er/Ho involves energy transfer $Er^{III} \rightarrow Ho^{III}$ processes.

All samples were synthesized by a solid state photochemical deposition method followed by a subsequent calcination process. The luminescent properties reveal that samples under 980 nm irradiation exhibit characteristic up-conversion emissions that are focused in the green region of the spectrum and that the nature of second activator (Ln) determines the degree of efficiency of these emissions.

1. Introduction

The up-conversion (UC) materials are a class of materials based in the conversion of light, by which the absorption of two or more low-energy photons (near infrared radiation) leads to the emission of one photon of high energy (visible radiation) [1–3] This type of materials generally comprise the inorganic host, sensitizer and activators. The choice of host lattice is an important factor in obtaining efficient up-conversion processes. The choice of the sensitizer and activators is obtained by the co-doping between two different lanthanide ions (Ln^{III}) into the host crystalline lattice with the purpose of exploiting the energy transfer UC process.

The Lanthanum oxide (La_2O_3) emerges as functional material due to their distinguished chemical, electrical and optical properties. Some of its optical properties include: long range of band gap 4.3–5.6 eV [4,5], long spectral range of transparency from visible to near infrared [4] and low phonon frequency of 400–600 cm^{-1} [6,7]. These properties are decisive in the choice of a host material for a wide variety of Ln^{III} ions as activators. The low phonon frequency might be propitious to promote emission, minimizing the energy loss due to non-radiative relaxations [8] and the wide band gap between valence and conduction bands endow it the capability to accommodate the energy level transition of most Ln^{III} ions [9]. On the other hand, the Ln^{III} ions can easily substitute in La^{III} lattice due to similar chemical properties, ionic radii and electronegativity of La^{III} resulting in high efficient optical properties [10].

In this contribution, we have proposed to study the influence of different additives (Nd or Ho) on the up-conversion emissions when these are co-doped with Er in La_2O_3 thin films. In this study, the co-doped samples (La_2O_3:Er-Ln) where Ln = Nd or Ho, show an increase in emission intensities. However, these emissions depend heavily on the type of additive used. The difference in the emissions is attributed to the different mechanistic routes that have been proposed.

2. Experimental details

2.1. Preparation of amorphous thin films

The precursor complexes lanthanum(III) tris(2,2,6,6-tetramethyl-3,5-heptanedionate), [La(tmhd)$_3$], erbium(III) tris(2,2,6,6-tetramethyl-3,5-heptanedionate), [Er(tmhd)$_3$], holmium(III) tris(2,2,6,6-tetramethyl-3,5-heptanedionate), [Ho(tmhd)$_3$] and neodymium(III) tris(2,4-pentanedionate), [Nd(acac)$_3$] were purchased from Sigma-Aldrich Chemical Company. The substrates for film deposition were quartz plates (2 × 2 cm^2) and n- and p-type silicon (100) wafers (1 × 1

* Corresponding author.
E-mail address: gcabello@ubiobio.cl (G. Cabello-Guzmán).

https://doi.org/10.1016/j.optmat.2019.109579
Received 24 September 2019; Received in revised form 12 November 2019; Accepted 26 November 2019
Available online 6 December 2019

cm^2), which were obtained from Wafer World Inc., Florida, USA.

For the deposition of La_2O_3 films, the $La(tmhd)_3$ complexes were homogenized in a CH_2Cl_2 solution. The thin films were prepared as follows. A silicon chip was placed on a spin-coater and rotated at a speed of 600 rpm. An aliquot (0.5 ml) of the precursor complex in CH_2Cl_2 solution was deposited onto the silicon chip and allowed to spread. The spin-coater motor was stopped after 60 s, and a thin film of the complex remained on the chip. The quality of the films was examined using optical microscopy (500x magnification).

For the deposition of La_2O_3:xEr-Ln films (Ln = Ho or Nd), solutions of $La(tmhd)_3$ with different proportions of $Er(tmhd)_3$ (where x = 5, 10 and 15 mol %) and a fixed portion in 10 mol % of $Ho(tmhd)_3$ or 10 mol % of Nd $(acac)_3$, were spin-coated on the appropriate substrate, and the thin films were irradiated until no absorption due to the complexes was observed in the infrared spectrum.

2.2. Photolysis of the complexes as films on Si(100) surfaces

All photolysis experiments were performed following identical procedures. First, the Fourier transform infrared spectroscopy (FT-IR) spectrum of the starting film was obtained. Then, the chip was placed under a UV-lamp setup that was equipped with two 254 nm 6 W tubes in air. The reaction progress was monitored by recording the FT-IR spectrum at different time intervals following a decrease in the IR absorption of the complexes. After the FT-IR spectrum showed no evidence of the starting material, the chip was rinsed several times with dry acetone to remove all remaining organic products on the surface prior to analysis. To obtain films with a specific thickness, successive layers of the precursor materials were deposited by spin-coating and irradiated as previously described. This process was repeated several times until the desired thickness was achieved. Post-annealing was performed under a continuous flow of synthetic air at different temperatures (350–950 °C) for 3 h in a programmable Lindberg tube furnace.

2.3. Characterization of the thin films

The FT-IR spectra were obtained with a 4 cm^{-1} resolution on a PerkinElmer Spectrum Two FT-IR spectrophotometer. The UV spectra were obtained with a 1 nm resolution on a PerkinElmer Model Lambda 25 UV–vis spectrophotometer. X-ray diffraction (XRD) patterns were obtained using a D8 Advance Bruker X-ray diffractometer; the X-ray source was Cu Kα radiation (40 kV/30 mA). X-ray photoelectron spectroscopy (XPS) was performed on an XPS-Auger PerkinElmer electron spectrometer Model PHI 1257 that included an ultra-high vacuum chamber, a hemispherical electron energy analyzer and an X-ray source that provided unfiltered Kα radiation from its Al anode ($h\nu$ = 1486.6 eV). The pressure of the main spectrometer chamber during data acquisition was maintained at approximately 10^{-7} Pa. The binding energy (BE) scale was calibrated using the peak of adventitious carbon, which was set to 284.6 eV. The accuracy of the BE scale was ±0.1 eV. The morphology and presence of elements in the samples were evaluated by scanning electron microscopy (SEM) with a Hitachi model SU 3500 with an accelerating voltage of 10.0 kV. SEM was coupled with Bruker model Quantax 100 energy dispersive X-ray spectroscopy (EDX) for semi-quantitative determinations.

The up-conversion luminescent properties were determined with a Hitachi F-7000 fluorescent spectrometer using a power-tunable 980 nm diode laser. All measurements were performed at room temperature.

3. Results and discussion

3.1. Evaluation of the photo-reactivity of the precursor complexes

Fig. 1 shows the absorption spectral changes corresponding to diluted concentrations ($\leq 10^{-5}$ mol/L) of each precursor complex, when they were exposed to UV illumination at 254 nm at different time intervals. The absorption band centered at 276 nm is associated to the π → π* electronic transition of a carbonyl group (C═O) of the β-diketone ligands. The similarity of the absorption spectra responds to a same ligand independent of the metallic specie of complex. It can be seen from spectra that the intensity of the absorption band gradually decreases after 88, 152 and 157 min of irradiation for the $La(tmhd)_3$, $Ho(tmhd)_3$ and $Nd(acac)_3$ complexes, respectively. The exposure times for a particular complex may vary depending on the type of solvent used and the intensity of the UV lamp light. In this case, the experimental parameters were the same for each precursor complex, so that the differences in the irradiation time are due to the chemical nature of each precursor or to its concentration in the solution. After having exposed to each precursor complex under UV illumination, it is observed that all absorption bands are substantially lost and no spectral evidence for the formation of intermediate species is found during the photochemical reaction. These results are consistent with other studies about the photoreactivity of other β-diketonate complexes [11–13], where the gradual fragmentation of the precursor complex, the release of the metal ion from the sphere of coordination of the complex and finally the photo-reduction of the metallic species is proposed.

Fig. 2 shows the FT-IR spectral changes associated with the solid state photolysis. Thin films of the complex $La(tmhd)_3$ and thin films of $La(tmhd)_3$ with different molar proportions of $Er(tmhd)_3$ and Ln (β-diketonate)$_3$ (where Ln = Ho or Nd) were deposited on Si(100) substrates by spin-coating and subsequently irradiated with a 254 nm UV source in aerated conditions. It is possible to observe a gradual decrease with time in the intensities of the main signal associated to the β-diketonate complexes. Previous to the irradiation on the films (t = 0), we can identify some bands between 1385 and 1570 cm^{-1} attributed to symmetric and anti-symmetric C═O stretching of the β-diketonate ligands. After 144 h of irradiation, the intensity of all bands attributed to the complex are significantly reduced and only minimal signals are observed. The only broad band remaining after irradiation between 1475 and 1370 cm^{-1} can be assigned to CO_3^{2-} formation as by-products from the photo-degradation of the precursor complexes.

3.2. Thermal treatment and preliminary characterization of the photo-deposited thin films

Fig. 3 shows the FT-IR spectra of photo-deposited films that were annealed at different temperatures (350, 650 and 950 °C) for a period of 3 h. The un-doped and doped samples with Erbium are exhibited as a representative example. For samples annealed at 350 °C, the absorptions between 3300 and 3700 cm^{-1}, are due to the stretching mode of OH groups, corresponding to structural OH and adsorbed H_2O in the samples. The strong bands between 1400 and 1490 cm^{-1} are assigned to the symmetric and asymmetric stretching vibrations of C═O groups in carbonate CO_3^{2-} species [14,15]. Probably under these conditions, the samples adopt a $La(OH)CO_3$ composition more than the formation of the oxide. We have obtained similar results in a previous work using a yttrium(III) β-diketonate complexes as a precursor for the formation of $Y(OH)CO_3$ [16]. The samples annealed at 650 °C show the same signals but decrease in intensity. It has been reported [14] that the thermal decomposition of $La(OH)CO_3$ to La_2O_3 takes two steps. First is the transformation from $La(OH)CO_3$ to LaO_2CO_3 and secondly the transformation from LaO_2CO_3 to La_2O_3. Under these conditions the samples annealed at 650 °C will probably adopt the LaO_2CO_3 intermediate phase formation. Finally, when the samples are treated at 950 °C, new signals appear between 485 and 990 cm^{-1}, the bands located in the range of 480–600 cm^{-1} can be attributed to the La–O stretching frequencies of the La_2O_3 which confirm the formation of crystalline La_2O_3 [14,17], and the bands located in the range of 900–990 cm^{-1} which can be identified as unidentately bound carbonate species [17]. In this way, it is possible to affirm preliminary that samples under these conditions are formed by a mixture of $La_2O_3/La_2O_2CO_3$.

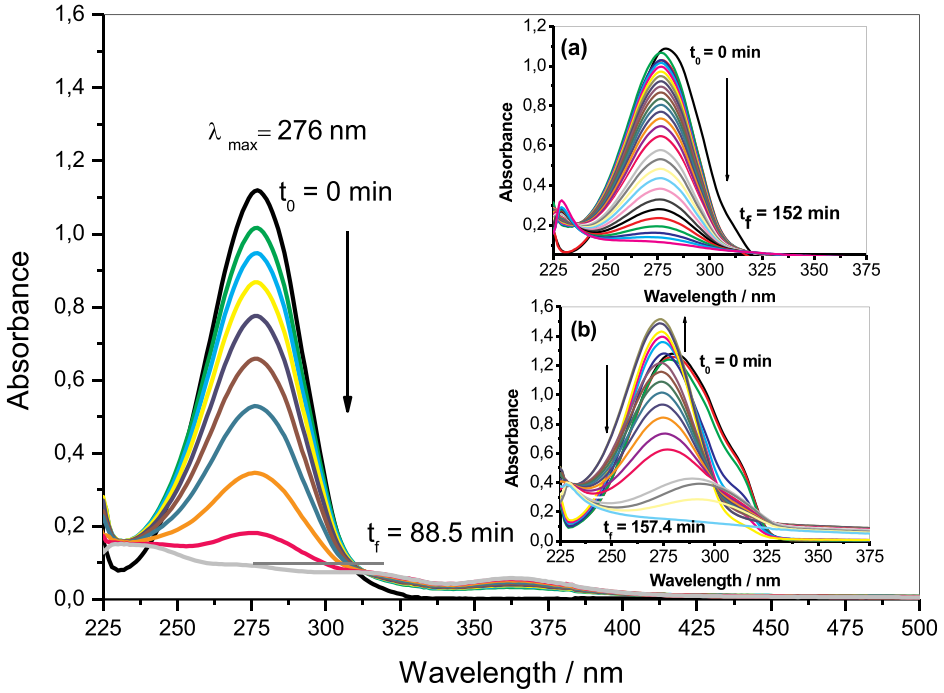

Fig. 1. Absorption spectral changes observed of a solution 1.56×10^{-6} mol/L of the La(tmhd)$_3$ complex in CH_2Cl_2 upon 88.5 min of UV irradiation (254 nm). Insets: **(a)** solution (3.78×10^{-5} mol/L) Ho(tmhd)$_3$ complex exposed to UV irradiation for 152 min, and **(b)** solution (4.52×10^{-5} mol/L) of the Nd(acac)$_3$ complex exposed at 157.4 min under irradiation with 254 nm light. The arrows indicate the sequence of the spectral evolution with time.

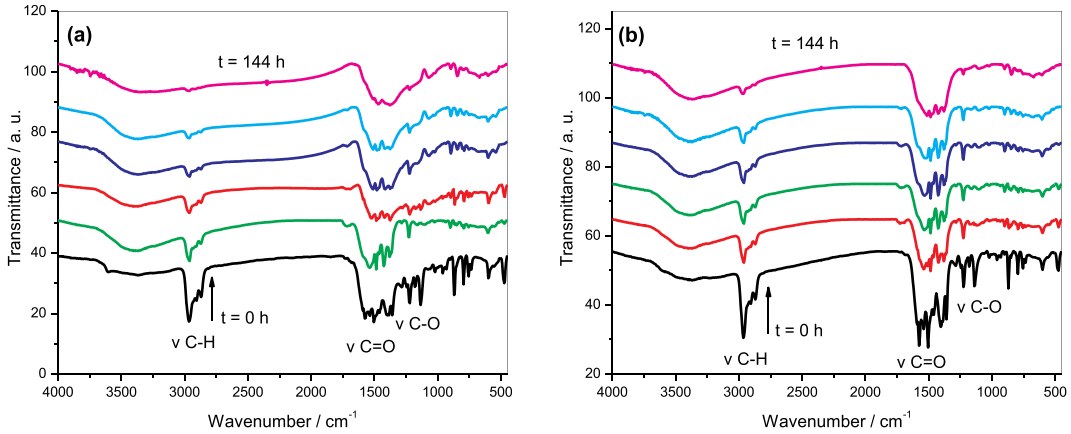

Fig. 2. FT-IR spectral changes accompanying the photolysis of films on Si(100) substrates of **(a)** La(tmhd)$_3$ and **(b)** La(tmhd)$_3$ with 15 mol % of Er(tmhd)$_3$ exposed to UV light for 0, 24, 48, 72, 96, 120 and 144 h.

3.3. Structure, chemical composition and morphology of annealed films

The XRD patterns of annealed La_2O_3 and La_2O_3 doped with Erbium at 950 °C are shown in Fig. 4. The diffractograms reveal that both samples exhibit the same pattern with two intense peaks associated to the (101) and (112) planes, assigned to the hexagonal phase La_2O_3 (JCPDS no 00-024-0554) [18]. It is observed that undoped La_2O_3 presents an additional plane in (100), which disappears in the doped sample La_2O_3:xEr (where x = 15 mol %), which can be attributed to the degree of incorporation of the additive into the crystalline lattice. One of the evidences to evaluate the degree of incorporation of an additive within the crystalline lattice of host material is the observation of a slight shift of the XRD peaks of the doped sample with respect to the position of the XRD signal of the pure sample. The inset in Fig. 4 shows the shift of the XRD peaks of the (101) and (112) lattice planes. The introduction of erbium as an additive in the crystalline lattice of La_2O_3 does not modify the intrinsic structure of the matrix but can alter the lattice parameters of the structure due to the differences in the ionic radius between the introduced additive and the substituted lanthanum ions in the crystalline lattice. It is known that the ionic radius of Er^{III} and La^{III} are 1.03 Å and 1.32 Å, respectively. Given that the ionic radius of the Er^{III} is slightly smaller than the ionic radius of the La^{III}, it is likely that a certain degree of substitution will occur. The substitution of La^{III} ions by smaller ions causes a slight shift towards higher 2θ values in the XRD peaks, causing a slight reduction of lattice size of the matrix [19]. However, a careful observation in the diffractograms reveals a very specific crystalline orientation given the appearance of some lattice planes that can be interpreted as a partial crystallization of the samples annealed at 950 °C. In this context, we think that a large part of the insertion of erbium into the matrix can occurs in the grain boundaries, in the interstices or dispersed over the deposit surface.

For the purpose of determining its chemical composition, the survey

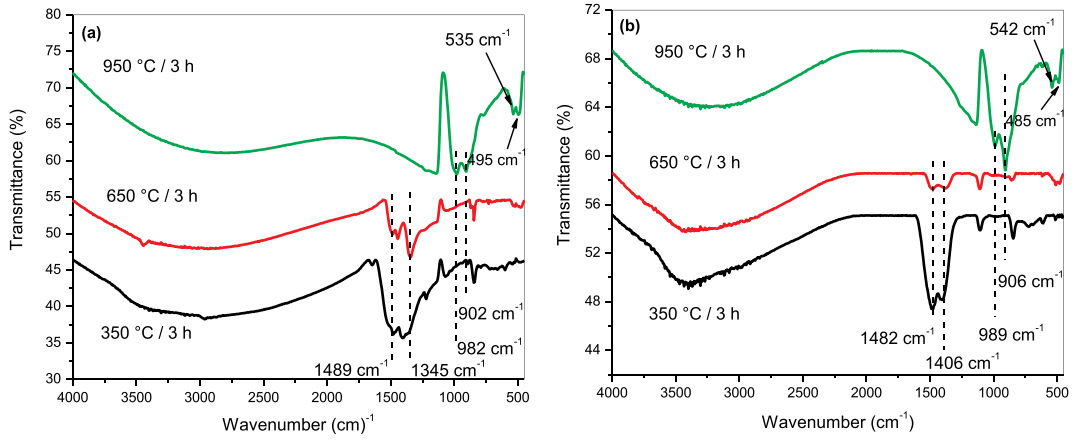

Fig. 3. FT-IR spectrum of the films photo-deposited and annealed at 350, 650 and 950 °C on silicon substrate **(a)** un-doped sample and **(b)** doped sample with 15 mol % of Er

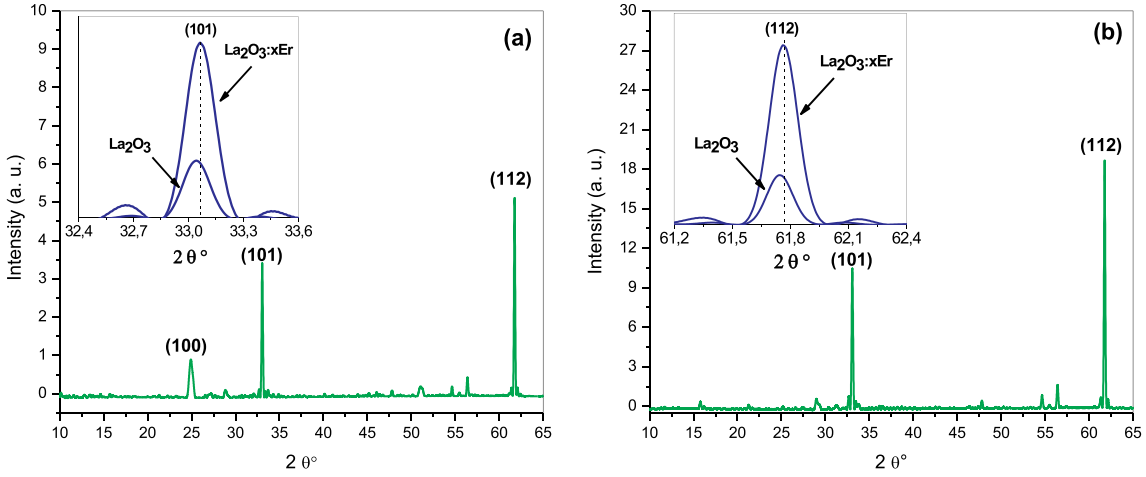

Fig. 4. XRD patterns of the annealed samples at 950 °C of **(a)** La_2O_3 and **(b)** La_2O_3 doped with 15 mol % of Er. The inset figures shows the shift of the diffraction peaks corresponding to (101) and (112) lattice planes, respectively.

XPS spectrum of the La_2O_3:Er films annealed at 950 °C was obtained. The spectrum (Fig. 5) shows the presence of La, O and Er in the samples. The La 3d spectrum shown In Fig. 6a, is split into two well separated spin orbit contributions with their respective satellites. Both contributions identified as La $3d_{3/2}$ at 852.5 eV and La $3d_{5/2}$ at 835.6 eV suggests the existence of La^{III} oxidation in the film. The energy difference of both signals ($\Delta E = 3d_{3/2} - 3d_{5/2} = 16.9$ eV) indicate the formation of lanthanum oxide [20,21]. The O 1s signal (Fig. 6, is determined by two contributions, one located at 531.0 eV assigned to lattice oxygen (La–O) and a second one located at 532.5 eV, associated to the ionization of oxygen species (O^{2-}) adsorbed on the surface or the presence of carbonated species (CO_3^{2-}) [18,22]. The Er 4d spectrum (not shown here) reveals a weaker and broad signal centered at 168.9 eV corresponding to the Er^{III} oxidation in the sample [23,24].

The morphology and elemental composition of the annealed samples were examined by SEM and EDS, respectively, as shown in Figs. 7–9. It can be seen from the SEM images in Fig. 7a (low magnification) and Fig. 7b (high magnification) that the La_2O_3 films have a microstructure with micro-sized particles randomly distributed but with some agglomerations on the surface of the substrate. The size of these agglomerations is variable and in a range of 6–10 μm with a distorted hexagonal aspect which is consistent with the results obtained by XRD. The composition of the constitutive elements (La and O) has been analyzed by EDS (Fig. 7c) and elemental mapping show that lanthanum and oxygen are homogeneously distributed over the surface in a compact

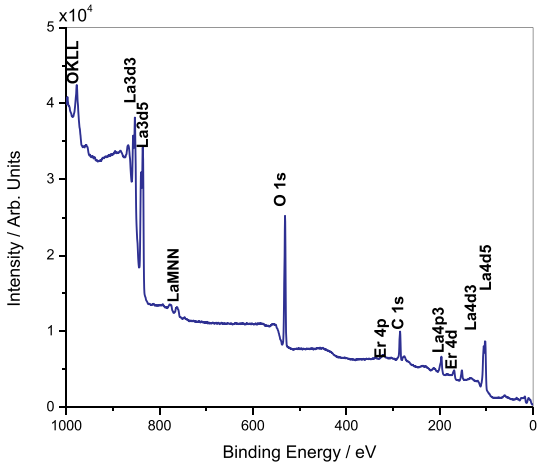

Fig. 5. XPS survey scan of the La_2O_3:xEr films photo-deposited and annealed at 950 °C for 3 h, where x = 15 mol% of erbium in the sample.

manner (Figs. 7d and e).

The morphological study was also applied to the co-doped samples (Er/Ho and Er/Nd) with the purpose of verifying the presence and superficial distribution of the additives in the films. In the case of the co-

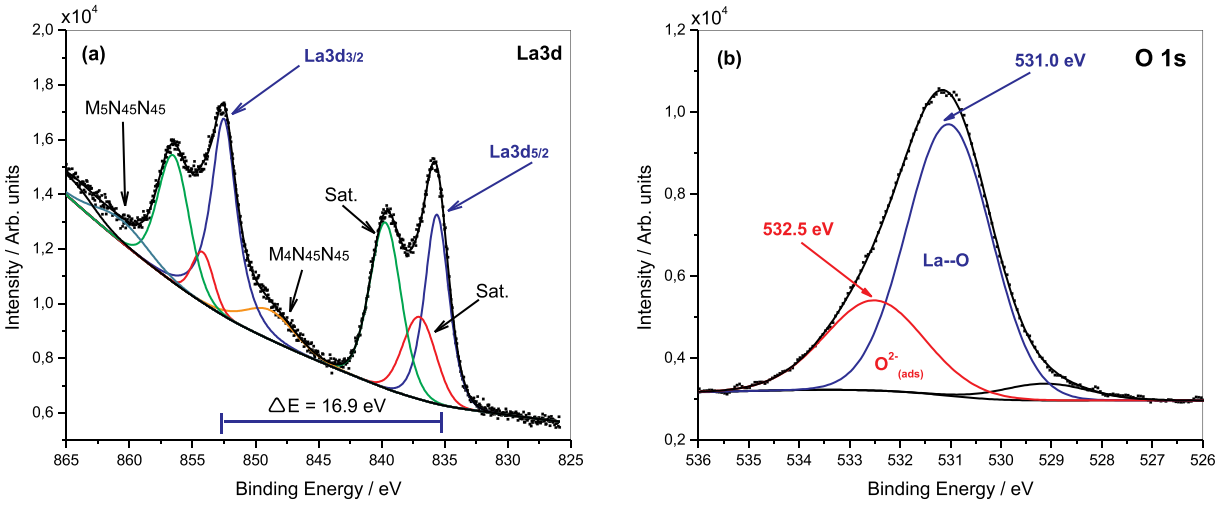

Fig. 6. High-resolution XPS spectra of the La_2O_3:xEr films photo-deposited and annealed at 950 °C **(a)** La 3d spectrum and **(b)** O 1s spectrum.

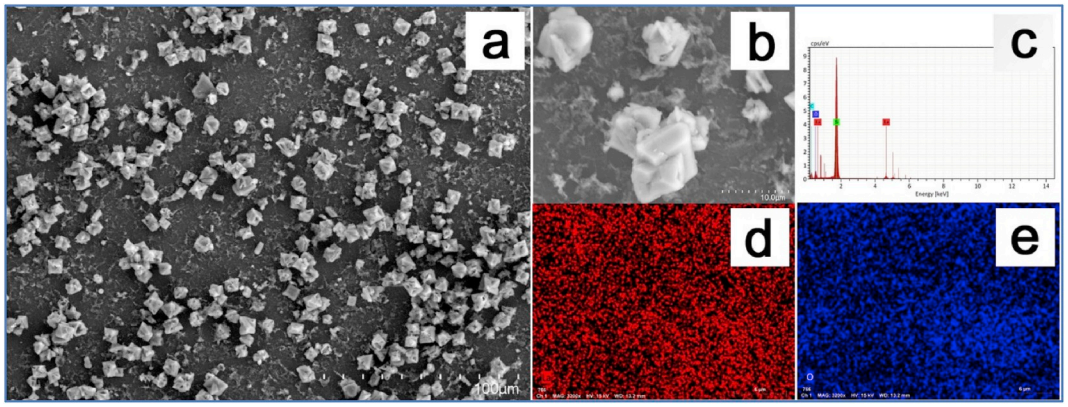

Fig. 7. SEM-EDS of La_2O_3 films annealed at 950 °C: **(a)** low-magnification SEM image; **(b)** high-magnification SEM image; **(c)** elemental composition from EDS spectra; **(d)** elemental mapping of lanthanum (red) and **(e)** elemental mapping of oxygen (blue) in the film. (For interpretation of the references to colour in this figure legend, the reader is referred to the Web version of this article.)

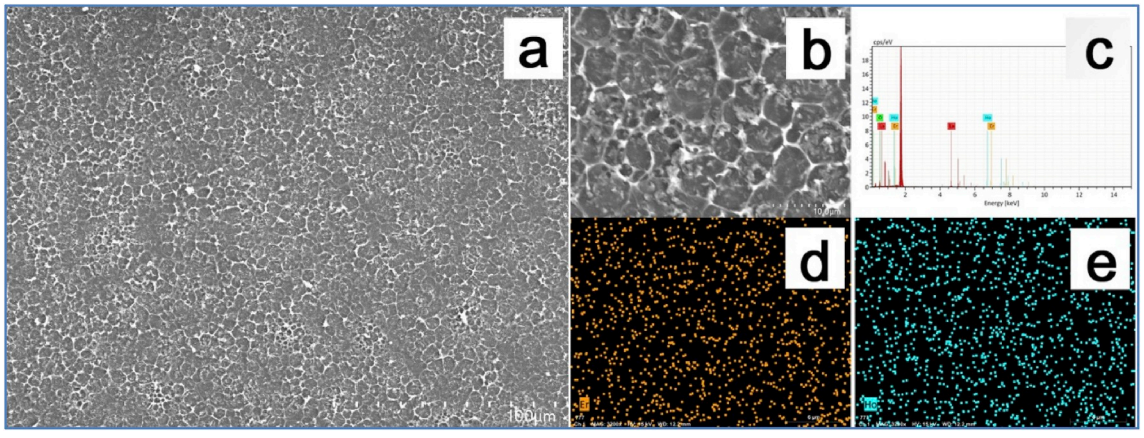

Fig. 8. SEM-EDS of La_2O_3:xEr-Ho films (where x = 10 mol % of each additive) annealed at 950 °C: **(a)** low-magnification SEM image; **(b)** high-magnification SEM image; **(c)** elemental composition from EDS spectra; **(d)** elemental mapping of erbium, and **(e)** elemental mapping of holmium in the film.

doped samples, a considerable change in the surface morphology is observed. As shown in Figs. 8a and b corresponding to the La_2O_3:xEr-Ho films, it is possible to observe an amorphous structure of fibrous characteristics but uniformly distributed throughout the surface. According to the results obtained by XRD it has been observed that the doping of the films tends to suppress some lattice planes in the XRD spectrum, probably by increasing the level of doping. In this particular case the co-doping of different lanthanide ions contributes to that the morphology of the film has a more amorphous appearance with a decrease in the degree of crystallinity of the samples. We suggest that the incorporation

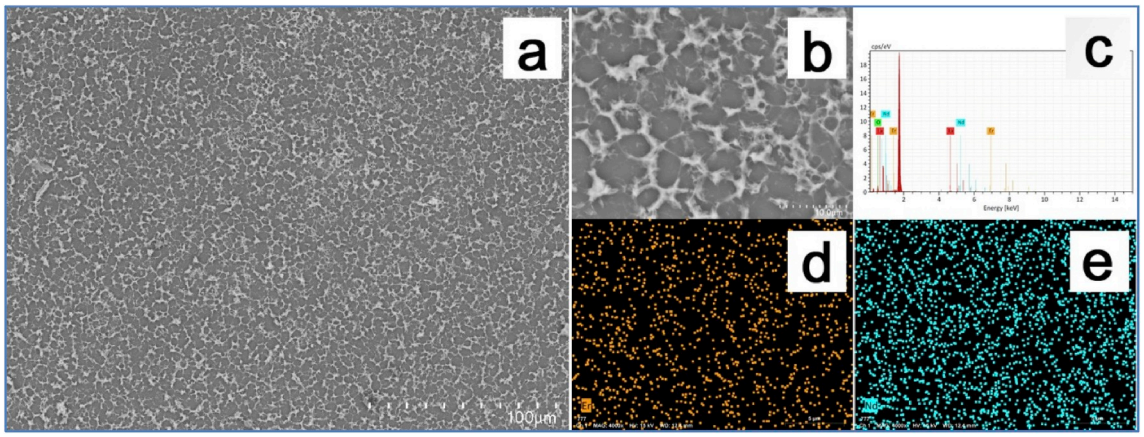

Fig. 9. SEM-EDS of the La_2O_3:xEr-Nd films (where x = 10 mol % of each additive) annealed at 950 °C: **(a)** low-magnification SEM image; **(b)** high-magnification SEM image; **(c)** elemental composition from EDS spectra; **(d)** elemental mapping of erbium, and **(e)** elemental mapping of neodymium in the film.

of ions with different ionic radius (Er(r) = 1.03 Å; Ho(r) = 0.901 Å and Nd(r) = 1.11 Å.) in a matrix can cause a certain degree of structural instability and gradually a loss of the crystalline nature of La_2O_3. Another possibility is that when generating the mixture between the precursor complexes for the photo-deposition of the matrix and their respective additives, a certain degree of incompatibility occurs, which hinders an adequate deposition and crystallization of the annealed samples. The EDS results (Fig. 8c) confirm the presence of La, O, Er and Ho. The elemental mapping of each additive shown in Figs. 8d and e demonstrates that the additives (Er/Ho) are distributed randomly over the entire surface of the sample.

Fig. 9 shows the morphology of the La_2O_3:xEr-Nd sample. The low-magnification (Fig. 9a) and high-magnification (Fig. 9b) images clearly indicates a rather amorphous aspect distributed evenly on the surface, very similar to the previous case. There are no significant morphological changes between the co-doped samples, in this way; the mixture of different precursor species in the photo-deposition and its subsequent thermal treatment hinders the formation of the nucleation sites in the formation of crystalline lattices. In Fig. 9c show the EDS spectra of the chemical composition of the La_2O_3:xEr-Nd film with the presence of La, O, Er and Nd. The examination by elemental mapping (Fig. 9d and e) shows that the additives (Er/Nd) are uniformly dispersed in the film. The results on the elemental composition of the un-doped and co-doped samples are exhibited in Table 1.

3.4. Optical properties of the films

The spectral transmittance characteristics of the samples annealed at 950 °C are shown in Fig. 10. In Fig. 10a presents the levels of transmittance as a function of the concentration of erbium as an additive. It is observed that all samples have two types of absorption at 208 and 242 nm that can ascribed to electronic transitions from the O 2p valence band to the La 5d6s conduction band of La_2O_3 and the transitions associated to defect states of lattice material, respectively [25]. A slight increase in transmittance across the spectrum (200–1000 nm) occurs when the level of doping increases. This phenomenon corresponds to that for experimental reasons in the deposition of the films; the doped samples presented a smaller thickness. A similar result has been obtained with the co-doped samples (see Fig. 10b), from these data the band gap (E_g) values are obtained applying the Tauc plot method [26] and these values are shown in the inset Fig. 10b. The E_g value obtained for the La_2O_3 was 4.46 eV, which increases slightly for doped and co-doped samples. This slight increase can be attributed to the amorphous nature of the films doped and co-doped as observed in the images by SEM.

Table 1
Elemental composition obtained from the EDS analysis of the samples annealed at 950 °C.

Film/ element	O–K atom %	La atom %	Er atom %	Ho atom %	Nd atom %	O/ La
La_2O_3	54.2	45.8	–	–	–	1.18
La_2O_3:xEr-Ho[a]	48.2	37.5	6.04	8.26	–	1.28
La_2O_3:xEr-Nd[a]	48.6	36.2	7.10	–	8.10	1.34

[a] where x = 10 mol % of each additive.

3.5. Up-conversion luminescence properties of the films

It has been observed [27,28] that Erbium ions inserted in different host materials present three typical emission bands at 510–530, 530–570 and 610–680 nm which correspond to the energy transfer of $^2H_{11/2} \rightarrow {}^4I_{15/2}$, $^4S_{3/2} \rightarrow {}^4I_{15/2}$, and $^4F_{9/2} \rightarrow {}^4I_{15/2}$, respectively, under excitation at 980 nm.

Fig. 11a shows the up-conversion emission spectra of La_2O_3:Er and La_2O_3:Er-Ln samples (Ln = Ho or Nd) observed under 980 nm laser excitation. A series of emission bands can be observed in the green spectral region centered at 540 nm ($^4S_{3/2} \rightarrow {}^4I_{15/2}$ transition) and in the red spectral region centered at 680 and 700 nm both signals have been assigned to $^4F_{9/2} \rightarrow {}^4I_{15/2}$ transition associated to the Er^{III} ions. In addition to these signals, a series of emission bands of varying intensity are also observed. These emissions are broad and overlap each other, very different from crystalline phosphors where the emission signals are sharp and fine as a consequence of Stark splitting [29]. It has been argued that energy positions of Stark levels and their oscillator strengths strongly depend on the local chemical environment (ligand field) and asymmetry at lanthanide ions site [30]. The variation of chemical environment in amorphous solids may induce the variation of Stark energy levels positions and consequently an alteration in the emission signals with respect to the luminescence of a crystalline solid. This characteristic shows that the material has a more amorphous appearance than a crystalline aspect.

The results show that gradually increasing the erbium concentration in the doped samples increases the emission intensity. However, when the second additive (Ho or Nd) is incorporated a significant increase of the erbium emissions is observed. In this way, energy transfer processes can take place contributing to the up-conversion emissions.

To explore the underlying mechanisms of co-doping induced up-conversion emission enhancement, we first determined the dependence of up-conversion luminescence intensity on pump power as shown in Fig. 11b revealing that the intensity of up-conversion luminescence

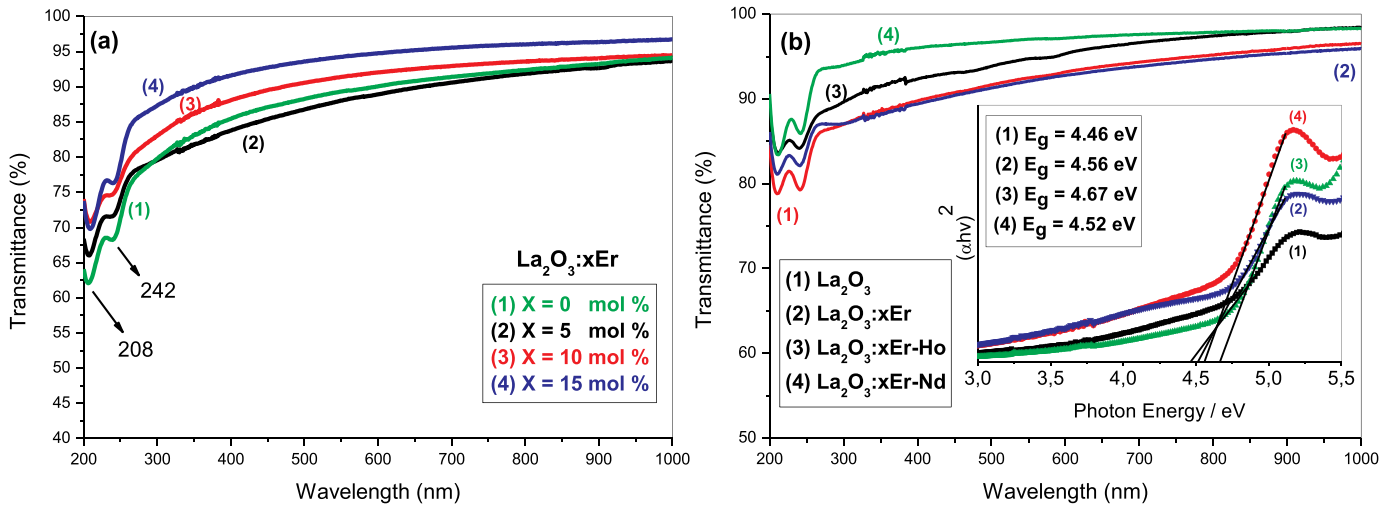

Fig. 10. Transmittance spectra for **(a)** La_2O_3 thin films doped with Erbium at different concentrations, where x = 0, 5, 10, and 15 mol % and **(b)** La_2O_3 pure, doped and co-doped thin films. The inset shows the optical band gap of the pure, doped and co-doped samples, determined according to Tauc plot method.

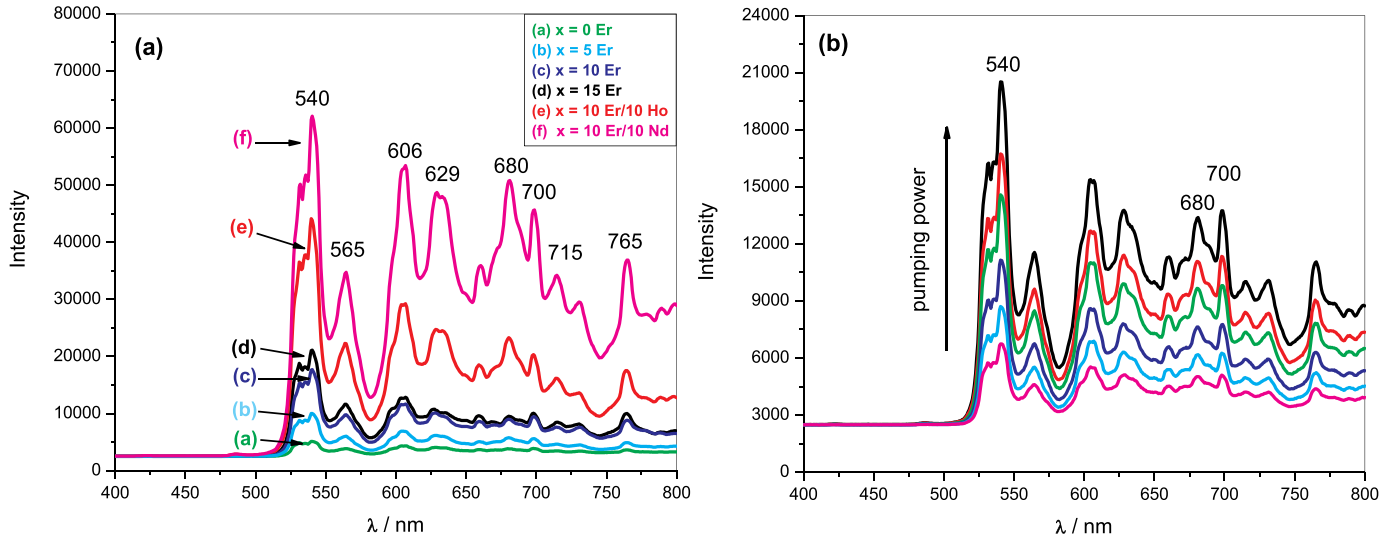

Fig. 11. Up-conversion emission spectra of **(a)** La_2O_3:xEr films, where x = 0, 5, 10 and 15 mol% of Er and La_2O_3:Er-Ln films, (where Ln = Ho or Nd) at 10 mol% of Er and 10 mol% of Ln. **(b)** The dependence of the up-conversion intensity on different excitation power levels of the La_2O_3:xEr sample (x = 15 mol% of Er).

increases with the increase of pump power.

The up-conversion luminescence intensity (I_{UC}) is proportional to the "*n*"th of excitation power (I_{IR}) according to the expression: $I_{UC} \sim I^n_{IR}$, where *n* is the number of absorbed NIR photons per visible photon emitted and can be obtained from slope (*n*) of $\ln(I_{UC})$ versus $\ln(I_{IR})$ analysis. In this way, the value of *n* must be close to 2 [31].

Fig. 12 reveals the logarithm plots of the emission intensity as a function of pump power for the green (540 nm) and red (680 nm, 700 nm) emissions respectively. For the green (540 nm) and red (680 and 700 nm) emissions, the values of the slope were determined to be 1.85, 1.63 and 1.65, respectively. These results show that the two photon process is responsible for up-conversion emissions.

To understand the enhancement mechanism, we evaluate the up-conversion emissions of the samples doped with Er. Fig. 13 shows that upon excitation at 980 nm, the Erbium ions are excited from their ground state ($^4I_{15/2}$) to an intermediate excited state ($^4I_{11/2}$) by a process known as ground state absorption (GSA). The energy stored in the $^4I_{11/2}$ level is again excited to a higher energy level ($^4F_{7/2}$) by a process known as excited state absorption (ESA). Both absorption processes (GSA and ESA), would explain the number of absorbed NIR photons per visible photon emitted in the doped samples. Both absorption processes can be explained by the values close to n ~2 obtained from the expression $I_{UC} \sim I^n_{IR}$. Continuing with the $^4F_{7/2}$ excited level of erbium ions, these decay non-radiatively to an intermediate energy level ($^4S_{3/2}$) and later decays radiatively to the ground state ($^4I_{15/2}$). This $^4S_{3/2} \rightarrow {}^4I_{15/2}$ transition is responsible for the green emission at 540 nm. On the other hand, the red emissions located at 680 and 700 nm, occur first by a non-radiative relaxation ($^4F_{7/2} \rightarrow {}^4F_{9/2}$) and then by a radiative decay assigned to $^4F_{9/2} \rightarrow {}^4I_{15/2}$ transitions.

The contribution of Nd^{III} ions in the co-doped samples (La_2O_3:Er/Nd) is observed by a considerable increase in emission intensities centered at 540 nm and to a lesser degree to red emissions centered at 680 and 700 nm. This behavior is probably due to the fact that the Nd^{III} ions are excited to the $^4F_{3/2}$ level from the ground sate ($^4I_{9/2}$) under excitation at 980 nm. The energy could then be transferred (ET) to Er^{III} ions and populate their $^4I_{11/2}$ states, resulting in a significant increase in the emissions of the Er^{III} ions through the ESA processes. Similar mechanisms involving energy transfer processes ($Nd^{III} \rightarrow Er^{III}$) to explain various luminescent emissions in different samples have been reported [32–34].

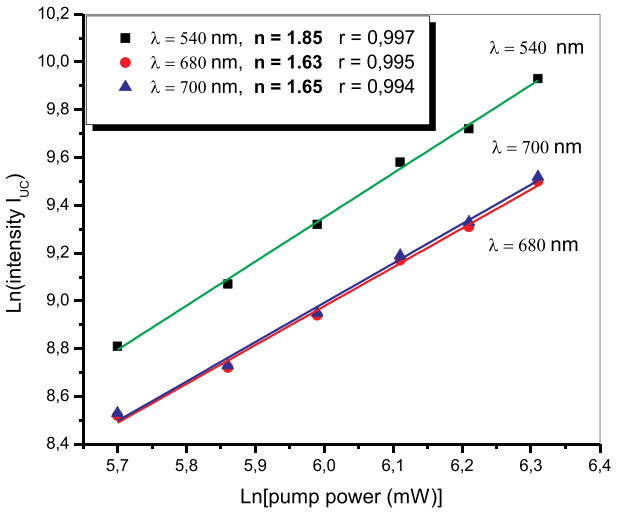

Fig. 12. Logarithmic (Ln) dependence of up-conversion luminescence intensity on laser power at 540, 680 and 700 nm emissions of the La_2O_3 doped with Er at 15 mol %. The *n* value denote the slope of the curve (number of absorbed NIR photons) and r the value of the linear correlation coefficient.

Traditionally, in the co-doping of various materials, Ho^{III} ions have been used mainly as activators due to their abundant electronic energy levels for the up-conversion luminescence. However, upon 980 nm excitation, the Ho^{III} ions have low emission intensity and pump efficiency because of their very low absorption cross-section [35]. This is why the use of sensitizers from other lanthanide ions which help to absorb the energy received and transferred to the activators through multiple-photon processes, have been proposed by several authors: Yb→Ho [36], Er→Ho [37]. It is known that Ho^{III} ions inserted as an additive have essentially two up-conversion emissions, one around 640–680 nm and another around 520–560 nm corresponding to the $^5F_5 \rightarrow {}^4I_8$ and $^5S_2, {}^5F_4 \rightarrow {}^5I_8$ electronic transitions, respectively [38].

In Fig. 11a it is shown the up-conversion emission spectra of La_2O_3: Er/Ho samples. It is observed that the signals increase in intensity compared to the doped samples (La_2O_3:Er) but are significantly less intense than in the La_2O_3:Er/Nd samples. Different luminescent evaluations with La_2O_3:Ho doped samples showed only emission predominantly centered in the green region at 538 nm assigned to $^5S_2, {}^5F_4 \rightarrow {}^5I_8$ transition of Ho^{III} ions, and no signals are observed from the red emission. However, this green emission at 538 nm is less intense and overlaps with the emission signal of the Er^{III} ions in the co-doped samples (La_2O_3: Er/Ho).

Under this context, assuming that Ho^{III} ions have poor absorption at 980 nm, the source of excitation is received primarily by Er^{III} ions through the GSA and ESA absorption processes, as previously mentioned and shown in Fig. 14. The energy stored at level $^4F_{7/2}$ of Er^{III} ions is transferred to levels $^5F_4$ ($^5S_2$) of Ho^{III} ions, in other words there is an energy transfer process ($Er^{III} \rightarrow Ho^{III}$). The energy received immediately translates into the emission of green from level $^5F_4$ to the basal state $^5I_8$ of Ho^{III} ions. This contribution could explain why the emission intensities in the green are more intense in the co-doped samples (La_2O_3: Er/Ho) with respect to the La_2O_3:Er samples.

However, the La_2O_3:Er/Ho samples have a lower intensity than their analogs (La_2O_3:Er/Nd), this behavior is due to the fact that the efficiency of the emissions falls on the Er^{III} ions. As has been observed, the samples co-doped with Er/Nd, both additives are excited and one of them

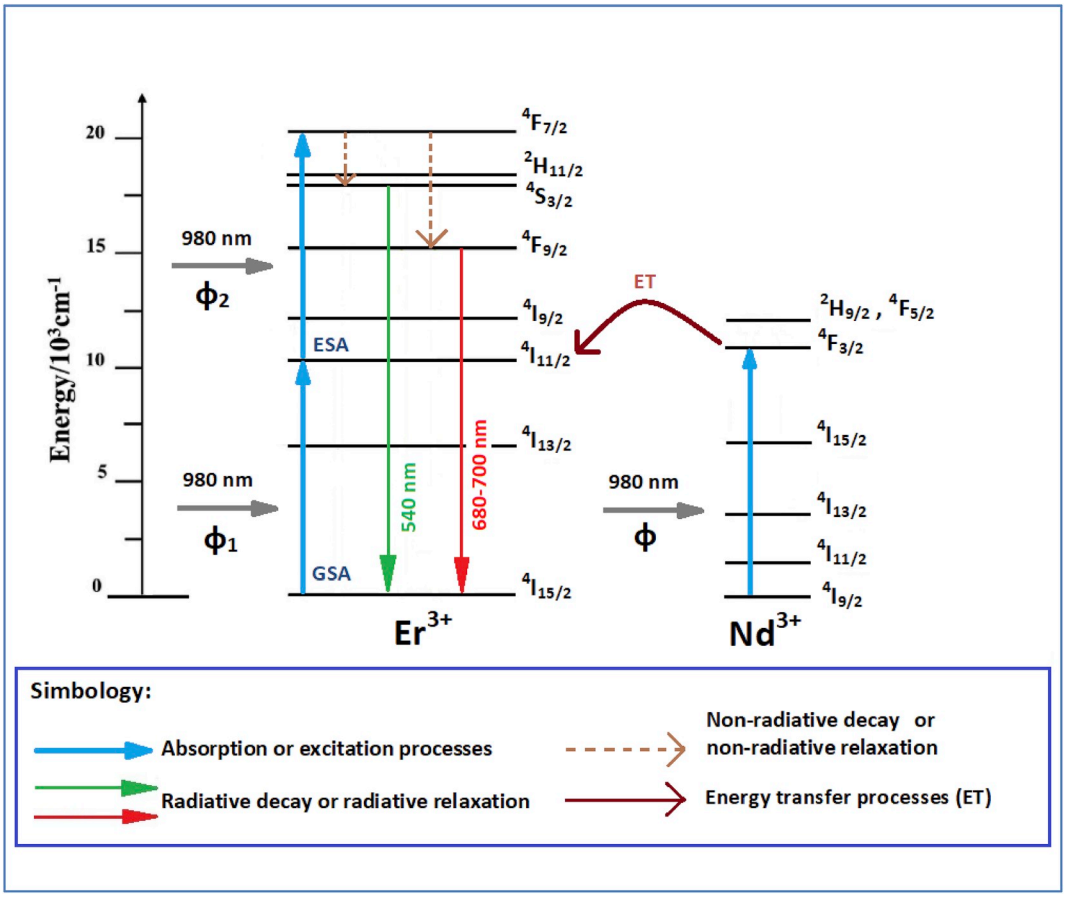

Fig. 13. Schematic representing of absorption modes (GSA and ESA) of Er ions and energy transfer (ET) processes from excited state of Nd ions to energy levels of Er ions with their respective emissions.

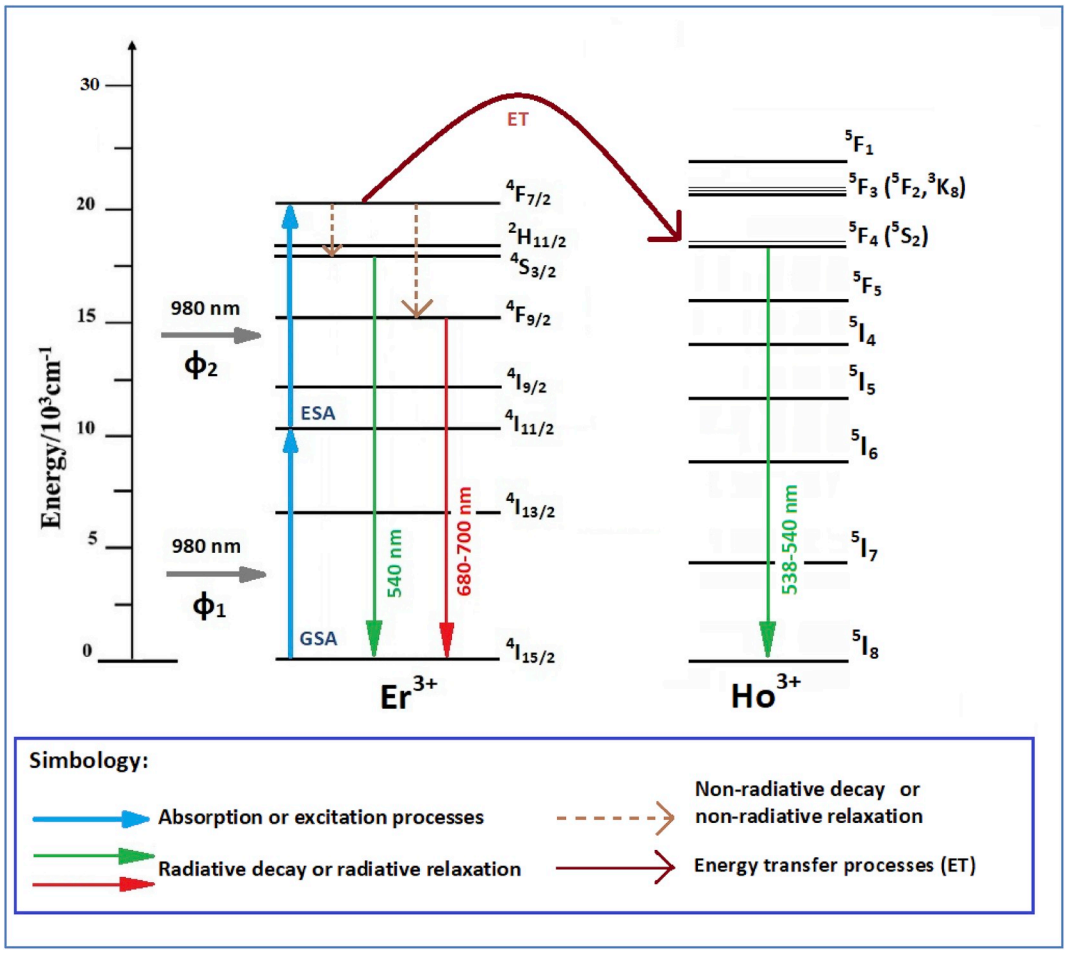

Fig. 14. Schematic representation of the absorption modes (GSA and ESA) of Er ions and their energy transfer (ET) processes from excited state of Er ions to energy levels of Ho ions and their respective emissions.

transfers its energy to the other ($Nd^{III} \rightarrow Er^{III}$) which means that emissions in the visible spectrum are attributed to Erbium ions (Fig. 13). While in the samples co-doped with Er/Ho the process is different, only the Erbium ions are excited and transfer some of their energy to the Ho^{III} ions emitting in the green region of the spectrum (Fig. 14).

Finally, according to the results obtained, the increase in up-conversion emissions through co-doping in a given material depends largely on the nature of the additives used.

4. Conclusions

La_2O_3 films doped with Er^{III} ions and co-doped with Nd^{III} and Ho^{III} were prepared by a simple photochemical method, followed by post-annealing at 950 °C. The elemental composition, morphology and phase formation were estimated using XPS, EDS-SEM and XRD measurement respectively. The results indicate that co-doped samples have amorphous characteristics, making it difficult to correlate the structure of the material with its optical properties.

Under 980 nm excitation of samples doped with Er^{III} ions, the up-conversion emissions were observed at 540 nm aprox. These emissions increase in intensity in the co-doped samples, due to energy transfer processes occurring from $Nd^{III} \rightarrow Er^{III}$ on one hand and from $Er^{III} \rightarrow Ho^{III}$ on the other. However, the type of mechanism involved in the proposed mechanism, contributes to explain why the emissions of the samples co-doped with Er/Nd are more intense than their analogous co-doped with Er/Ho. Subsequent studies incorporating the emissions lifetimes and structural studies of the samples will confirm the proposed mechanism.

Finally, in light of these results, it is observed that although the co-doping of lanthanide ions on La_2O_3 matrices contributes to an increase of the up-conversion emissions, the incorporation and nature of the second activator determines the degree of efficiency of the emissions.

Author contributions section

G. Cabello Guzmán: Conceptualization; Methodology; Supervision; Project administration; Funding acquisition and Writing - Original Draft.
C. Caro Díaz: Investigation and Validation.
A. Fernandez-Perez: Investigation and Validation.
G.E. Buono-Core: Resources and Writing - Review & Editing.
B. Chornik: Investigation and Validation.

Declaration of competing interest

The authors declare that they have no known competing financial interests or personal relationships that could have appeared to influence the work reported in this paper.

Acknowledgments

The authors are grateful to the CONICYT-FONDEQUIP-Chile Program (No EQM-140088) for the acquisition of the Hitachi Scanning Electron Microscope (SEM). We are grateful to the Research Office at the University of Bío-Bío, project DIUBB No 181109-4/R and to CONICYT-FONDECYT Program (National Fund for Scientific and Technological Development), Chile, Grant No 1190357, for financial support.

The authors adhere to the social movement unleashed in Chile in the

citizen demand for a new constitution that guarantees equity and social justice.

References

[1] Lei Yin Ang, Meng Earn Lim, Li Ching Ong, Yong Zhang, Applications of upconversion nanoparticles in imaging, detection and therapy, Nanomedicine 6 (7) (2011) 1273–1288.

[2] Ling-Dong Sun, Hao Dong, Pei-Zhi Zhang, Chun-Hua Yan, Upconversion of rare earth nanomaterials, Annu. Rev. Phys. Chem. 66 (2015) 619–642.

[3] Tomasz Grzyb, Artur Tyminski, Up-conversion luminescence of GdOF:Yb^{3+}, Ln^{3+} (Ln= Ho, Tm, Er) nanocrystals, J. Alloy. Comp. 660 (2016) 235–243.

[4] Romeo Singh Loitongbam, N. Shanta Singh, W. Rameshwor Singh, R. S. Ningthoujam, Observation of exceptional strong emission transitions ^5D_j (j= 1-3) to ^7F_j (j= 1-3): multicolor from single Eu^{3+} ion doped La_2O_3 nanoparticles, J. Lumin. 134 (2013) 14–23.

[5] R. Jbeli, A. Boukhachem, I. Ben Jemaa, N. Mahdhi, F. Saadallah, H. Elhouichet, S. Alleg, M. Amlouk, H. Ezzaouïa, An enhancement of photoluminescence property of Ag doped La_2O_3 thin films at room temperature, Spectrochim. Acta, Part A 184 (2017) 71–81.

[6] Guangrun Chen, Ruoshan Lei, Shiqing Xu, Huanping Wang, Shilong Zhao, Feifei Huang, Tian Yin, Effect of Li^+ ion concentration on upconversion emission and temperature sensing behavior of La_2O_3:Er^{3+} phosphors, J. Rare Earths 36 (2018) 119–124.

[7] Neha Jain, Rajan Kr Singh, Srivastava Amit, S.K. Mishra, Jai Singh, Prominent blue emission through Tb^{3+} doped La_2O_3 nano-phosphors for white LEDs, Physica B 538 (2018) 70–73.

[8] A. Siai, P. Haro-Gonzalez, K. Horchani-Naifer, M. Ferid, La_2O_3:Tm,Yb,Er upconverting nano-oxides for sub-tissue lifetime thermal sensing, Sens. Actuators, B 234 (2016) 541–548.

[9] Li Liang, Xiyan Zhang, Zhaohui Bai, Weili Dong, Hui Shi, Qingxue Xue, Preparation and near-infrared luminescence properties of Y_2O_3:Er^{3+}, Yb^{3+} nanopowders, Infrared Phys. Technol. 73 (2015) 49–53.

[10] N. Pushpa, M.K. Kokila, N.J. Shivaramu, Luminescence properties of La_2O_3:Eu^{3+} nanophosphor prepared by sol–gel method, Nucl. Instrum. Methods Phys. Res., Sect. B 379 (2016) 69–72.

[11] Salvatore Giuffrida, L. Lucia, Costanzo, Giorgio Ventimiglia, Corrado Bongiorno, Photochemical synthesis of copper nanoparticles incorporated in poly(vinyl pyrrolidone), J. Nanoparticle Res. 10 (2008) 1183–1192.

[12] B. Marciniak, G.E. Buono-Core, Photochemical properties of 1,3-diketonate transition metal chelates, J. Photochem. Photobiol., A 52 (1) (1990) 1–25.

[13] Salvatore Giuffrida, G. Guglielmo, Lucia L. Costanzo Condorelli, Giorgio Ventimiglia, Raffaella Lo Nigro, Maria Favazza, Enrico Votrico, Corrado Bongiorno, Ignazio L. Fragala, Nickel nanostructured materials from liquid phase photodeposition, J. Nanoparticle Res. 9 (2007) 611–619.

[14] Zhenhe Xu, Shasha Bian, Jiaqi Wang, Tao Liu, Liming Wang, Yu Gao, Preparation and luminescence of La_2O_3:Ln^{3+} (Ln3+ = Eu^{3+}, Tb^{3+}, Dy^{3+}, Sm^{3+}, Er^{3+}, Ho^{3+}, Tm^{3+}, Yb^{3+}/Er^{3+}, Yb^{3+}/Ho^{3+}) microspheres, RSC Adv. 3 (2013) 1410–1419.

[15] Zhenhe Xu, Qian Zhao, Yaguang Sun, Baoyi Ren, Lixin You, Shuju Wang, Dinga Fu, Synthesis of hollow La_2O_3:Yb^{3+}/Er^{3+}/Tm^{3+} microspheres with tunable up-conversion luminescence properties, RSC Adv. 3 (2013) 8407–8416.

[16] G. Cabello-Guzmán, Diego González, C. Caro-Díaz, L. Lillo-Arroyo, F. Valenzuela-Melgarejo, G. Cárdenas Triviño, G.E. Buono-Core, B. Chornik, Preliminary evaluation of the up-conversion emission of Y_2O_3:Er-Yb thin films prepared by a solid state photochemical deposition method, J. Lumin. 204 (2018) 401–409. Yosselin Huentupil.

[17] Minna Nieminen, Matti Putkonen, Lauri Niinisto, Formation and stability of lanthanum oxide thin films deposited from β-diketonate precursor, Appl. Surf. Sci. 174 (2001) 155–165.

[18] A.A. Yadav, A.C. Lokhande, J.H. Kim, C.D. Lokhande, Enhanced sensitivity and selectivity of CO gas sensor based on modified La_2O_3 nanorods, J. Alloy. Comp. 723 (2017) 880–886.

[19] Bhanu P. Gangwar, Sanat Chandra Maiti, Sudhanshu Sharma, Modifying the hygroscopic property of La_2O_3 by Pr, Sm and Nd doping, J. Solid State Chem. 256 (2017) 109–115.

[20] S.B. Brachetti-Sibaja, S.E. Rodil, M.A. Domínguez-Crespo, A.M. Torres-Huerta, E. Rodríguez, A.B. López-Oyama, Optical properties of nanocrystalline La_2O_3 dielectric films deposited by radio frequency magnetron sputtering, Thin Solid Films 636 (2017) 615–621.

[21] Milon Miah, Shatabda Bhattacharya, Diptiman Dinda, Shyamal K. Saha, Temperature dependent supercapacitive performance in La_2O_3 nanosheet decorated reduce graphene oxide, Electrochim. Acta 260 (2018) 449–458.

[22] A.A. Yadav, A.C. Lokhande, R.B. Pujari, J.H. Kim, C.D. Lokhande, The synthesis of multifunctional porous honey comb-like La_2O_3 thin film for supercapacitor and gas sensor applications, J. Colloid Interface Sci. 484 (2016) 51–59.

[23] Gurpreet Singh, Virpal, Ravi Chand Singh, Highly sensitive gas sensor based on Er-doped SnO_2 nanostructures and its temperature dependent selectivity towards hydrogen and ethanol, Sens. Actuators, B 282 (2019) 373–383.

[24] Yufei Tang, Cong Wu, Song Yuan, Yuanlin Zheng, Kang Zhao, Synthesis and luminescence properties of Er-doped and Er/Yb-codoped $CoAl_2O_4$ pigments, Ceram. Int. 44 (2018) 12909–12916.

[25] Huang Qing Liu, LingLing Wang, Weiqing Huang, ZhiWei Peng, Preparation and luminescence properties of nanocrystalline La_2O_3:Eu phosphor, Mater. Lett. 61 (2007) 1968–1970.

[26] Gang Gaoa, Yangc Lei, Bing Dai, Fei Xia, Zhenhuai Yang, Shuai Guo, Peng Wang, Fangjuan Geng, Jiecai Han, Jiaqi Zhu, Investigation of the effect of annealing temperature on optical properties of lanthanum-oxide thin films prepared by sol-gel method, Surf. Coat. Technol. 365 (2019) 164–172.

[27] Hongyu Li, Qianwen Huang, Yangbo Wang, Kun Chen, Juan Xie, Yue Pan, Haiquan Su, Xiaoji Xie, Ling Huang, Wei Huanga, Sc^{3+} – induced morphology, phase structure, and upconversion luminescence evolution of YF_3:Yb/Er nanocrystals, J. Mater. Chem. C. 5 (2017) 6450–6456.

[28] M. Pokhrel, G.A. Kumar, C.-G. Ma, M.G. Brik, Brian W. Langloss, Ian N. Stanton, Michael J. Therien, D.K. Sardar, Yuanbing Mao, Electronic and optical properties of Er-doped Y_2O_2S phosphors, J. Mater. Chem. C. 3 (2015) 11486–11496.

[29] S.V. Eliseeva, J.-C.G. Bünzli, Lanthanide luminescence for functional materials and bio-sciences, Chem. Soc. Rev. 39 (2010) 189–227.

[30] Dianna Himics, Lukas Strizik, Jiri Oswald, Holubova Jana, Ludvik Benes, Slang Stanislav, Bozena Frumarova, Tomas Wagner, 1.2 μm and 1.5 μm near-infrared photoluminescence and visible upconversion photoluminescence in GeGaS:Er^{3+}/Ho^{3+} glasses under 980 nm excitation, J. Mater. Sci. Mater. Electron. 29 (2018) 17314–17322.

[31] Jingning Shan, Mruthunjaya Uddi, Robert Wei, Nan Yao, Yiguang Ju, The hidden effects of particle shape and criteria for evaluating the upconversion luminescence of the lanthanide doped nanophosphors, J. Phys. Chem. C 114 (2010) 2452–2461.

[32] Pratik Deshmukh, S. Satapathy, Anju Ahlawat, M.K. Tiwari, A.K. Karnal, Fabrication and characterization of Er, Nd codoped Y_2O_3 transparent ceramic: a dual mode photoluminescence emitter, J. Alloy. Comp. 754 (2018) 32–38.

[33] Yingjie Shao, Qiuhong Yang, Yan Gui, Ye Yuan, Qing Lu, Spectroscopic properties of Er/Nd co-doped yttrium lanthanum oxide transparent ceramics pumped at 980 nm, J. Alloy. Comp. 667 (2016) 76–81.

[34] Yunyun Liu, Yijian Sun, Yan Wang, Zhenyu You, Zhaojie Zhu, Jianfu Li, Chaoyang Tu, Benefit of Nd^{3+} ions to the ~2.7 μm emission of Er^{3+}: $^4I_{11/2}$→$^4I_{13/2}$ transition in Nd,Er: $CaLaGa_3O_7$ laser crystal, J. Lumin. 198 (2018) 40–45.

[35] Jia Zhang, Jianming Jia, Morphologies and up-conversion luminescence of $Gd_4O_3F_6$:RE^{3+} (RE= Yb, Er, Ho and Tm) phosphors by hydrothermal synthesis, J. Lumin. 174 (2016) 1–5.

[36] Yuwaraj K. Kshetri, Bhupendra Joshi, Tae-Ho Kim, Soo Wohn Lee, Blue, green, red and near-infrared emissions via upconversion in α-sialon, Mater. Lett. 199 (2017) 147–150.

[37] Yuwaraj K. Kshetri, Bhupendra Joshi, Soo Wohn Lee, Intense visible upconversion emission in transparent (Ho^{3+}, Er^{3+})-α-Sialon ceramics under 980 nm laser excitation, J. Eur. Ceram. Soc. 36 (2016) 4215–4224.

[38] Hom Nath Luitel, Rumi Chand, Takanori Watari, $CaMoO_4$:RE^{3+},Yb^{3+},M^+ phosphor with controlled morphology and color tunable upconversion, Displays 42 (2016) 1–8.